A fast and sensitive new satellite SO_2 retrieval algorithm based on principal component analysis: Application to the ozone monitoring instrument

Can Li,[1,2] Joanna Joiner,[2] Nickolay A. Krotkov,[2] and Pawan K. Bhartia[2]

[1]   We describe a new algorithm to retrieve SO_2 from satellite-measured hyperspectral radiances. We employ the principal component analysis technique in regions with no significant SO_2 to capture radiance variability caused by both physical processes (e.g., Rayleigh and Raman scattering and ozone absorption) and measurement artifacts. We use the resulting principal components and SO_2 Jacobians calculated with a radiative transfer model to directly estimate SO_2 vertical column density in one step. Application to the Ozone Monitoring Instrument (OMI) radiance spectra in 310.5–340 nm demonstrates that this approach can greatly reduce biases in the operational OMI product and decrease the noise by a factor of 2, providing greater sensitivity to anthropogenic emissions. The new algorithm is fast, eliminates the need for instrument-specific radiance correction schemes, and can be easily adapted to other sensors. These attributes make it a promising technique for producing long-term, consistent SO_2 records for air quality and climate research. **Citation:** Li, C., J. Joiner, N. A. Krotkov, and P. K. Bhartia (2013), A fast and sensitive new satellite SO_2 retrieval algorithm based on principal component analysis: Application to the ozone monitoring instrument, *Geophys. Res. Lett.*, *40*, doi:10.1002/2013GL058134.

1.   Introduction

[2]   Sulfur dioxide (SO_2) is an important pollutant gas that can have profound impacts on the Earth's environment. It is a designated criteria air pollutant in many countries, and also a precursor of sulfate aerosols that can significantly affect air quality and climate [e.g., *Charlson et al.*, 1992]. With a relatively short atmospheric lifetime, the average surface concentration of SO_2 spans several orders of magnitude between polluted and pristine regions [*Chin et al.*, 2000]. On the other hand, from time to time, sizable transient SO_2 plumes can travel into remote oceanic areas [e.g., *Hsu et al.*, 2012]. Given this large inhomogeneity in its distribution, it is imperative to develop capabilities of measuring SO_2 globally with good accuracy and precision over relatively small spatial and temporal scales.

Additional supporting information may be found in the online version of this article.

[1]Earth System Science Interdisciplinary Center, University of Maryland, College Park, Maryland, USA.

[2]NASA Goddard Space Flight Center, Greenbelt, Maryland, USA.

Corresponding author: C. Li, Earth System Science Interdisciplinary Center, University of Maryland, College Park, MD 20742, USA. (can.li@nasa.gov)

[3]   Satellite measurements of global SO_2 pollution have undergone substantial improvements over the past 10–15 years owing to the launch of several hyperspectral UV-Visible instruments. Among them is the Ozone Monitoring Instrument (OMI), a Dutch-Finnish sensor flying on NASA's Aura spacecraft that provides daily global coverage at high spatial resolution ($13 \times 24 \, km^2$ at nadir) [*Levelt et al.*, 2006]. The operational OMI level-2 (L2) planetary boundary layer (PBL) SO_2 data are produced using the Band Residual Difference (BRD) method that utilizes three selected wavelength pairs to maximize sensitivity to PBL pollution [*Krotkov et al.*, 2006]. While useful for monitoring strong anthropogenic sources [e.g., *Fioletov et al.*, 2011; *Li et al.*, 2010], the OMI PBL SO_2 product suffers from the effects of random instrument noise as well as systematic biases [e.g., *Lee et al.*, 2009]. A background correction and multiyear pixel averaging can help to mitigate these issues but may introduce new biases and restrict the time resolution of data analyses [*Streets et al.*, 2013]. Other methods, such as the Iterative Spectral Fitting (ISF) algorithm [*Yang et al.*, 2009], have had some success improving the quality of OMI SO_2 retrievals [e.g., *He et al.*, 2012]. Operational implementation of the ISF algorithm, however, has proved difficult owing to the amount of computation involved in the radiative transfer calculations for many wavelengths, and the empirical corrections required to remove retrieval artifacts.

[4]   In this study, we introduce a fundamentally different approach to retrieve SO_2 from OMI-measured radiance and irradiance data. Our method is based on principal component analysis (PCA), a statistical technique often employed to reduce dimensionality while retaining the information content of a multivariate data set, by transforming it into a subspace spanned by a set of orthogonal vectors (principle components, PCs). PCA has been applied to compress data and retrieve temperature and moisture profiles from high-resolution infrared satellite instruments [e.g., *Huang and Antonelli*, 2001]. *Guanter et al.* [2012] and *Joiner et al.* [2013] used PCA-based approaches to retrieve terrestrial chlorophyll fluorescence from satellite and ground-based spectral data. As demonstrated below, our algorithm shares a similar general framework with these approaches and can significantly improve the quality of OMI SO_2 retrievals as compared with the current operational PBL product.

2.   Methodology

2.1.   General Framework

[5]   To illustrate our approach, we start from the widely used differential optical absorption spectroscopy (DOAS) method for trace gas retrievals. If there are n gases with absorption cross sections $\sigma_g(\lambda)$ at a given wavelength λ, the Sun-normalized Earthshine radiance at the top of the atmosphere (TOA),

$I(\lambda)/I_0(\lambda)$, can be modeled with the weak absorption Beer-Lambert law [e.g., *Platt and Stutz*, 2008] as

$$ln\left(\frac{I(\lambda)}{I_0(\lambda)}\right) = -\sum_{g=1}^{n} S_g\sigma_g(\lambda) - P(\lambda) - \text{RRS}(\lambda), \quad (1)$$

where $I(\lambda)$ and $I_0(\lambda)$ are the Earthshine radiance and solar irradiance at TOA, respectively, S_g is the number density of gas g along the optical path (slant column density, SCD), $P(\lambda)$ is a polynomial term representing broadband effects including atmospheric Rayleigh and aerosol/cloud Mie scattering and surface reflectance, and $\text{RRS}(\lambda)$ is a term to account for the rotational-Raman scattering (also known as the Ring effect). S_g can be estimated through least squares fitting that minimizes the differences between the measured and modeled radiance spectra (i.e., left- and right-hand sides of equation (1)). It may then be converted to a vertical column density (Ω_g or VCD) with an estimate of the air mass factor (AMF). The AMF is typically calculated at a single wavelength based on a prescribed vertical profile of gas g along with other assumptions.

[6] Uncertainties in the DOAS fitting can arise from inaccurate modeling of the various physical processes in equation (1) as well as artifacts in the radiance measurements (e.g., stray light). For example, the rotational-Raman effect is very difficult to model accurately in the SO₂-relevant spectral window since it involves the filling-in of both telluric and solar lines and is sensitive to cloud properties. The measurement artifacts often require the addition of an effective absorber term in the fitting, but modeling of them can also be quite complicated and may or may not fit the formulation in equation (1). As with the DOAS method, the BRD and ISF algorithms also rely on empirical, instrument-specific corrections to the radiance data in order to reduce retrieval noise and biases.

[7] Instead of attempting to model all these various factors, we propose to replace them with characteristic features derived directly from the measured Sun-normalized radiances. In this algorithm, the PCA technique is applied to the radiance data to extract a set of PCs that capture most of measurement-to-measurement variation of the radiances (in the absence of the signal of interest). For our problem, we may use data from a region presumed free of SO₂ (e.g., the equatorial Pacific). Then, the derived PCs will capture physical and measurement details other than those associated with SO₂ absorption. The PCs are ordered so that the first PC explains the most of variance, the second PC explains the second most of variance, and so on. A set of n_v PCs (v_i) can be used along with the sensitivity of the radiances to the SO₂ column (SO₂ Jacobians, $\partial N/\partial\Omega_{\text{SO}_2}$) to form a forward model:

$$N(\omega, \Omega_{\text{SO}_2}) = \sum_{i=1}^{n_v} \omega_i v_i + \Omega_{\text{SO}_2}\frac{\partial N}{\partial\Omega_{\text{SO}_2}}, \quad (2)$$

where N is a measured N value spectrum ($N(\lambda) = -100 \times \log_{10}$ $(I(\lambda)/I_0(\lambda))$). For polluted regions with actual SO₂ signals, the forward model can be inverted through standard least squares fitting to simultaneously retrieve the VCD of SO₂ (Ω_{SO_2}) and the coefficients of the PCs (ω). Note that an assumption here is that a linear combination of PCs calculated from SO₂-free regions can well describe the non-SO₂ affected radiances in SO₂-polluted areas. In most cases this assumption should hold true given the relatively weak absorption by SO₂ outside of

polluted regions. The use of SO₂ Jacobians for the entire fitting window also removes the step for converting SCD to VCD using an AMF.

2.2. Application to the OMI Instrument

[8] OMI level 1B (L1B) radiance and irradiance data in the spectral window of 310.5–340 nm were used in this study, together with the VCD of O₃ (Ω_{O_3}) from the L2 OMTO3 product [*Bhartia and Wellemeyer*, 2002]. This spectral window includes the strong SO₂ absorption band at 310.8 nm and minimizes potential interferences due to stray light at shorter wavelengths. Our experiments also showed that the inclusion of wavelengths > 340 nm had no discernible impacts on retrievals. To better account for the orbit-to-orbit measurement artifacts, we analyzed data from one orbit at a time. Because the 60 cross-track positions (rows) of OMI are individual detectors (and essentially different instruments), we also treated each row of each orbit separately and filtered out pixels with slant column O₃ (S_{O_3}) > 1500 DU (Dobson unit, 1 DU = 2.69 × 10¹⁶ molecules/cm²); large S_{O_3} can diminish the measurement sensitivity to SO₂. S_{O_3} was calculated from Ω_{O_3}, the solar zenith angle (θ_0), and the viewing zenith angle (θ),

$$S_{\text{O}_3} = \Omega_{\text{O}_3}(\sec(\theta_0) + \sec(\theta)). \quad (3)$$

[9] After data screening, about 900–1300 pixels of various cloud fractions remained in each row for the PCA. We tested a few different sets of input spectra for generating the PCs: (1) the N value spectra, (2) the N value spectra normalized against 340 nm, and (3) the N value spectra after a fitted second-order polynomial were subtracted from each spectrum. As the retrievals of SO₂ were generally very similar for these different PCAs, hereafter we focus on the first method.

[10] Given the presence of transient SO₂ plumes, one challenge is how to differentiate between SO₂-free and SO₂-polluted regions. We note that for the vast majority of pixels, SO₂ absorption is normally not strong enough to cause significant changes in the radiances. It is thus unlikely for the PC(s) associated with or affected by SO₂ absorption (v_{SO2}) to be among the first few leading PCs, even if PCA is conducted on an entire row without first screening out polluted scenes. As long as n_v is sufficiently small to exclude v_{SO2} from equation (2), reasonable initial estimates of SO₂ ($\Omega_{\text{SO2\_ini}}$) can be obtained. A second step PCA can then be applied to pixels with small $\Omega_{\text{SO2\_ini}}$ (in this study the threshold was set at ±1.5 standard deviations for each orbit/row) to extract a new set of PCs to update equation (2), followed by updated retrievals of SO₂. This step can be repeated. We found that the changes in the retrieved SO₂ generally became very small within two iterations. We conducted the second step PCA and retrievals for three segments of each row: a "tropical" region with S_{O_3} < 100 DU + min(S_{O_3}), and two regions north and south of it. The resulting PCs for each segment more closely matched the measurements than the PCs acquired using the entire row. The use of these regionally derived PCs reduced retrieval biases.

[11] Another important consideration is how to determine n_v, the number of PCs to use in equation (2). Too few PCs will lead to large biases in SO₂ while too many may cause over fitting. Our test results indicated that in most cases, at least 20–30 PCs were necessary, while occasionally in the
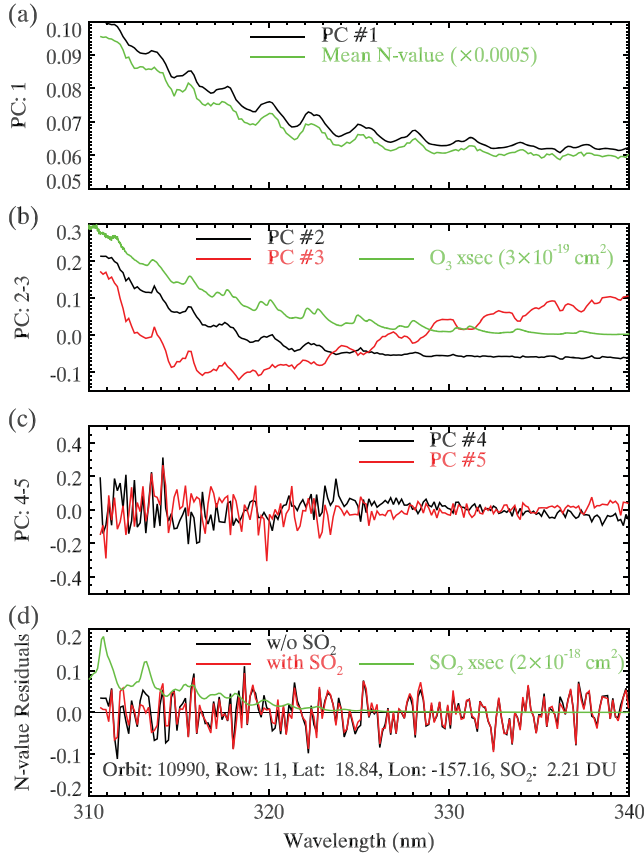
Figure 1. (a) The first PC extracted from the radiance data from row 11 of orbit 10,990, which passed over the Pacific on 08 August 2006. (b) The second and third PCs from the analysis. (c) The fourth and fifth PCs from the analysis. (d) The fitting residuals for a pixel near Hawaii presumably influenced by a volcanic plume. The red and black lines represent the fitting residuals with and without the SO$_2$ absorption term in equation (2), respectively. The estimated SO$_2$ VCD from the fitting is 2.21 DU. The green lines in Figures 1a, 1b, and 1d show the mean N value spectrum of the row, the O$_3$ and SO$_2$ cross sections both at 243 K, respectively. All units are in N values unless otherwise specified.

presence of relatively strong SO$_2$ signals, no more than 8 PCs could be used. Instead of using a constant n_v, we determined it for each row by checking the correlation between PCs (after the fifth) and the SO$_2$ Jacobians. For example, if significant correlation at the 95% confidence level existed between the ith PC and SO$_2$ Jacobians, only the preceding i-1 PCs would be included. We found this to be an effective way to prevent the inclusion of v_{SO2} and collinearity in equation (2). To maintain computational efficiency, an upper limit of 30 was set for n_v. The differences in SO$_2$ due to the use of a greater upper limit (e.g., 50) were found to be marginal, especially for polluted areas.

[12] The VLIDORT radiative transfer code [*Spurr*, 2008] was employed to calculate SO$_2$ Jacobians. To facilitate the comparison between the new algorithm and the operational PBL product, we used the same fixed atmospheric profiles as in the operational algorithm, and also assumed the same surface albedo (0.05), surface pressure (1013.25 hPa), fixed solar zenith angle (30°), and viewing zenith angle (0°). For SO$_2$, a climatological profile over the summertime eastern

U.S. was used. For O$_3$ and temperature, the OMTO3 standard midlatitude profiles with $\Omega_{O3} = 325$ DU were used. Details can be found in *Krotkov et al*. [2006]. In the future, we plan to expand the look-up table for SO$_2$ Jacobians to more realistically account for different measurement conditions. It should also be noted that while the PCA was conducted for pixels of all-sky conditions, we focus on relatively cloud-free scenes in the following sections, given that the calculated SO$_2$ Jacobians are not suitable for cloudy conditions.

3. Results

[13] As an example, Figures 1a–1c show the typical first few leading PCs extracted from the N value spectra of an entire row. The first PC essentially represents the mean spectrum of all the pixels. The second PC closely follows the spectral feature of the O$_3$ cross section, suggesting that O$_3$ absorption is a dominant contributor to the variance in the window. The third PC may be related to the surface contribution. It is difficult to assign a well-defined geophysical meaning to the fourth, the fifth, and the following PCs, but they probably reflect the rotational-Raman effect or various measurement artifacts such as the wavelength shift between radiance and irradiance spectra. The residuals from two different least squares fittings for a pixel near Hawaii are also shown in Figure 1d. While the same set of 30 PCs were used in both fittings, only one (red line) included the SO$_2$ Jacobians. As can be seen from the figure, the inclusion of SO$_2$ Jacobians had little effects at wavelengths > 320 nm, but substantially reduced the residuals in the strong SO$_2$ absorption bands at 310.8 and 313 nm. The initial estimate of SO$_2$ in the pixel was 2.21 DU, implying the influence of a nearby volcano.

[14] Figure 2 compares the global monthly mean SO$_2$ for August 2006 from the PCA algorithm and the operational OMI L2 PBL SO$_2$ product. The new algorithm largely reduces the systematic biases in the operational data, removing
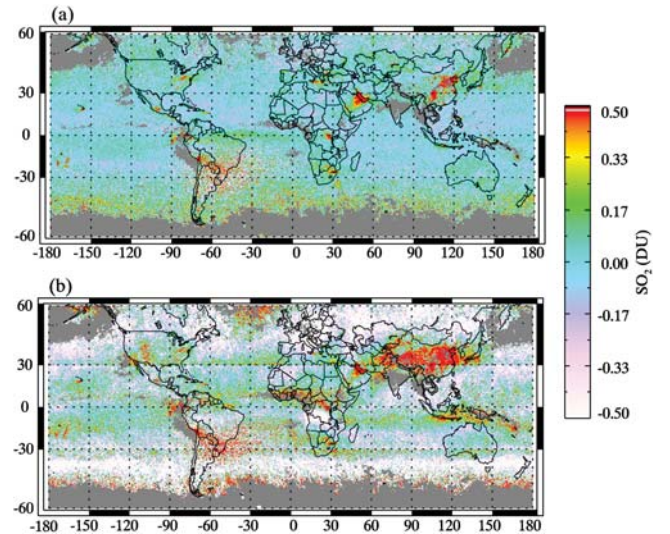
Figure 2. (a) Monthly mean SO$_2$ for August 2006 retrieved using the PCA algorithm. Data were gridded to 0.25° × 0.25°. Pixels outside the center 50 rows, or with radiative cloud fraction > 0.3 or slant column O$_3$ > 1500 DU were excluded. Gray-shaded grid cells have less than five measurements during the month. (b) Same as in Figure 2a but for the operational OMI L2 PBL SO$_2$ data.
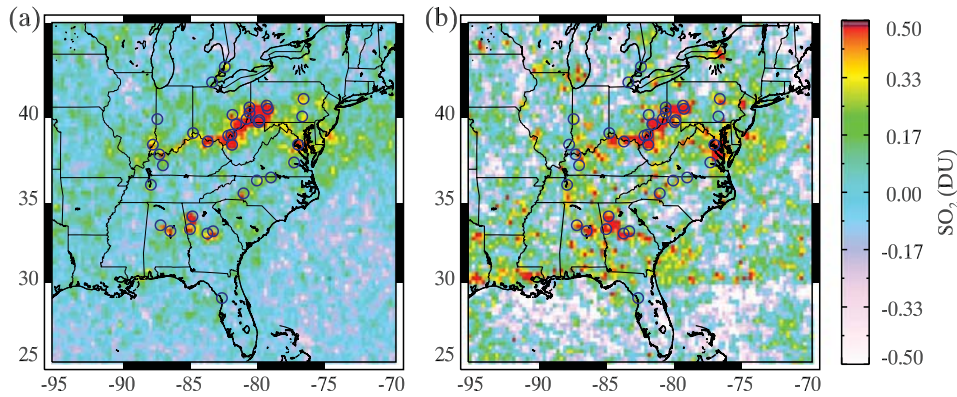
Figure 3. (a) The monthly mean SO$_2$ for August 2006 over the eastern U.S. retrieved using the PCA algorithm. Solid circles mark the locations of some major SO$_2$ point sources (> 70 kt/yr). (b) Same as in Figure 3a but for the operational OMI L2 PBL SO$_2$ product. Smaller stationary SO$_2$ sources may also be detected by the PCA algorithm, but likely will require data averaging over a longer period of time.

the step changes along 30°N and 30°S (probably related to the O$_3$ profile shape change in the OMTO3 algorithm), the positive values over the Tibet Plateau and the Rocky Mountains, and also the large negative values at higher latitudes. Meanwhile, the major known SO$_2$ source regions including eastern China, the eastern U.S., Mexico City, the industrial region in South Africa, as well as various degassing volcanoes are clearly discernible in the new retrievals. The SO$_2$ plume in the South Pacific (20°S, 170°W) was from the submarine eruption of the Home Reef volcano in Tonga that started on 07 August 2006. A close-up look at the eastern U.S. (Figure 3) further reveals the improvements made in the new algorithm. With reduced noise and biases, the large point sources in the region, such as the power plants in the Ohio River valley, Atlanta, and mid-Atlantic coast can be more clearly distinguished. More regional examples are provided in the supporting information. In some cases, the PCA algorithm may potentially be employed to monitor SO$_2$ pollution at higher temporal resolutions, as shown in the daily and weekly SO$_2$ maps also available in the supporting information.

[15] The mean and standard deviation of the PCA SO$_2$ and the operational OMI PBL SO$_2$ were calculated for the equatorial Pacific (10°S–10°N, 120°W–150°W) to compare the noise levels of the two retrievals (Table 1). For this presumably SO$_2$-free region, the standard deviation of PCA-retrieved SO$_2$ is ~0.5 DU, half that of the operational OMI product (~1.0 DU). The day-to-day variation of the mean PCA-retrieved SO$_2$ over the region (between −0.03 and 0.02 DU) is also smaller than that of the operational product (between −0.14 and 0.09 DU).

The improvements in the PCA retrievals are likely due to the use of more wavelengths and better characterization of orbit-to-orbit measurement artifacts (e.g., due to small changes in uncorrected detector dark currents).

4. Discussion and Future Work

[16] In summary, we have developed a new SO$_2$ retrieval algorithm based on principal component analysis of satellite-measured radiance data. Preliminary application of the new algorithm to OMI suggests that it can greatly reduce systematic biases in the current operational OMI PBL SO$_2$ data, and it suppresses the retrieval noise by a factor of 2. Our approach takes advantage of the fact that usually only a small portion of each satellite orbit has discernible SO$_2$ absorption signals, and data from the rest of the orbit can be used to characterize and extract other physical and measurement details. While also relying on the least squares fitting of the measured radiances, our method differs from the DOAS approach in that its forward model contains basis functions mostly derived from the data, instead of various precalculated reference spectra. This decreases the uncertainties associated with modeling and instrumental errors and speeds up the calculation. With much less computation required, the new PCA algorithm is much faster than the full spectral fit and requires only about 4–5 min to process an entire OMI orbit using a single state-of-the-art CPU.

[17] Another advantage of our PCA-based algorithm is that it largely eliminates the need to develop specific, empirical

Table 1. The Statistics of the PCA-Retrieved and the OMI Operational PBL SO$_2$ Over the Equatorial Pacific (10°S–10°N, 120°W–150°W) in August 2006[a]

Date[b]	Number of Pixels	PCA SO$_2$ Mean (DU)	PCA SO$_2$ SD (DU)	Operational Mean (DU)	Operational SD (DU)
08/01	10034	−0.002	0.511	0.059	0.949
08/06	8823	0.006	0.512	0.010	0.994
08/11	7056	0.017	0.501	−0.033	1.015
08/16	7007	0.030	0.507	−0.053	0.945
08/21	8299	−0.009	0.486	−0.043	0.937
08/26	9538	−0.017	0.498	0.000	0.952
08/31	9838	−0.012	0.504	0.060	0.946
Range[c]		−0.020 to 0.030	0.484 to 0.561	−0.140 to 0.094	0.929 to 1.064

[a]Data outside the center 50 rows, or with radiative cloud fraction > 0.3 or slant column O$_3$ > 1500 DU excluded.
[b]Dates are formatted as month/day.
[c]Minimal and maximal values for the entire month.

corrections to the radiance data for each instrument. Rather, measurement artifacts are accounted for by the PCs directly extracted from the radiance data. This reduces the potential artifacts/biases introduced by instrument-specific data correction schemes. The algorithm can be easily adapted to other satellite sensors, and this feature makes it particularly useful for building long-term, consistent SO$_2$ data records. In fact, we have tested the algorithm on the Ozone Mapping and Profiler Suite (OMPS) nadir mapping instrument flying on the Suomi National Polar-orbiting Partnership satellite. Using the algorithm with minimal changes (the only major change being the use of instrument-specific slit functions for SO$_2$ Jacobians), we achieved very consistent, high quality SO$_2$ retrievals from both OMI and OMPS.

[18] Next, we plan to expand the calculations of SO$_2$ Jacobians to account for different viewing geometries, surface albedo, and O$_3$ and SO$_2$ profiles. This is expected to further reduce retrieval noise and biases especially for oceanic regions. We will also more thoroughly evaluate the data quality, including an analysis of error propagation to estimate retrieval errors due to measurement noise. For data validation, the PCA retrievals will also be compared to existing airborne SO$_2$ measurements over the U.S. and China, as well as other data sources. Finally, we will investigate the possibility of applying the algorithm to other trace gas species. Some trace gases (e.g., HCHO) have fairly inhomogeneous spatial distributions similar to SO$_2$ and could be suitable for the approach.

References

Bhartia, P. K., and C. W. Wellemeyer (2002), OMI TOMS-V8 Total O$_3$ Algorithm, *Algorithm Theoretical Baseline Document: OMI Ozone Products*, edited by P. K. Bhartia, vol. II, ATBD-OMI-02, version 2.0, available at http://eospso.gsfc.nasa.gov/sites/default/files/atbd/ATBD-OMI-02.pdf.

Charlson, R. J., S. E. Schwartz, J. M. Hales, R. D. Cess, J. A. Coakley, J. E. Hansen, and D. J. Hofmann (1992), Climate forcing by anthropogenic aerosols, *Science*, *255*, 423–430.

Chin, M., R. B. Rood, S.-J. Lin, J. F. Muller, and A. M. Thompson (2000), Atmospheric sulfur cycle in the global model GOCART: Model description and global properties, *J. Geophys. Res.*, *105*, 24,671–24,687.

Fioletov, V. E., C. A. McLinden, N. Krotkov, M. D. Moran, and K. Yang (2011), Estimation of SO$_2$ emissions using OMI retrievals, *Geophys. Res. Lett.*, *38*, L21811, doi:10.1029/2011GL049402.

Guanter, L., C. Frankenberg, A. Dudhia, P. E. Lewis, J. Gómez-Dans, A. Kuze, H. Suto, and R. G. Grainger (2012), Retrieval and global assessment of terrestrial chlorophyll fluorescence from GOSAT space measurements, *Remote Sens. Environ.*, *121*, 236–251.

He, H., et al. (2012), SO$_2$ over central China: Measurements, numerical simulations and the tropospheric sulfur budget, *J. Geophys. Res.*, *117*, D00K37, doi:10.1029/2011JD016473.

Hsu, N. C., C. Li, N. A. Krotkov, Q. Liang, K. Yang, and S.-C. Tsay (2012), Rapid transpacific transport in autumn observed by the A-train satellites, *J. Geophys. Res.*, *117*, D06312, doi:10.1029/2011JD016626.

Huang, H.-L., and P. Antonelli (2001), Application of principal component analysis to high-resolution infrared measurement compression and retrieval, *J. Appl. Meteorol.*, *40*(3), 365–388.

Joiner, J., L. Guanter, R. Lindstrot, M. Voigt, A. P. Vasilkov, E. M. Middleton, K. F. Huemmrich, Y. Yoshida, and C. Frankenberg (2013), Global monitoring of terrestrial chlorophyll fluorescence from moderate-spectral-resolution near-infrared satellite measurements: Methodology, simulations, and application to GOME-2, *Atmos. Meas. Tech.*, *6*, 2803–2823.

Krotkov, N. A., S. A. Carn, A. J. Krueger, P. K. Bhartia, and K. Yang (2006), Band residual difference algorithm for retrieval of SO$_2$ from the AURA Ozone Monitoring Instrument (OMI), *IEEE Trans. Geosci. Remote Sens.*, *44*, 1259–1266.

Lee, C., R. V. Martin, A. van Donkelaar, G. O'Byrne, N. Krotkov, A. Richter, L. G. Huey, and J. S. Holloway (2009), Retrieval of vertical columns of sulfur dioxide from SCIAMACHY and OMI: Air mass factor algorithm development, validation, and error analysis, *J. Geophys. Res.*, *114*, D22303, doi:10.1029/2009JD012123.

Levelt, P. F., G. H. J. van den Oord, M. R. Dobber, A. Malkki, H. Visser, J. de Vries, P. Stammes, J. Lundell, and H. Saari (2006), The Ozone Monitoring Instrument, *IEEE Trans. Geosci. Remote Sens.*, *44*(5), 1093–1101, doi:10.1109/TGRS.2006.872333.

Li, C., Q. Zhang, N. A. Krotkov, D. G. Streets, K. He, S.-C. Tsay, and J. F. Gleason (2010), Recent large reduction in sulfur dioxide emissions from Chinese power plants observed by the Ozone Monitoring Instrument, *Geophys. Res. Lett.*, *37*, L08807, doi:10.1029/2010GL042594.

Platt, U., and J. Stutz (2008), *Differential Optical Absorption Spectroscopy, Principles and Applications*, Physics of Earth and Space Environments, vol. 15, pp. 597, Springer, Berlin Heidelberg, ISBN 978-3-540-21193-8.

Spurr, R. (2008), *LIDORT and VLIDORT: Linearized Pseudo-Spherical Scalar and Vector Discrete Ordinate Radiative Transfer Models for use in Remote Sensing Retrieval Problems*, Light Scattering Reviews, vol. 3, edited by A. Kokhanovsky, Springer, Berlin Heidelberg, doi:10.1007/978-3-540-48546-9.

Streets, D. G., et al. (2013), Emissions estimation from satellite retrievals: A review of current capability, *Atmos. Environ.*, *77*, 1011–1042.

Yang, K., N. A. Krotkov, A. J. Krueger, S. A. Carn, P. K. Bhartia, and P. F. Levelt (2009), Improving retrieval of volcanic sulfur dioxide from backscattered UV satellite observations, *Geophys. Res. Lett.*, *36*, L03102, doi:10.1029/2008GL036036.